International Journal of Computational and Experimental Science and ENgineering (IJCESEN)

Vol. 10-No.4 (2024) pp. 763-774
http://www.ijcesen.com

ISSN: 2149-9144

Research Article

Hybrid Deep Learning Based Model for Removing Grid-Line Artifacts from Radiographical Images

U. S. Pavitha[1,*], S. Nikhila[2], Mamtha Mohan[3]

[1]Assistant Professor, Department of Electronics and Communication Engineering, Ramaiah Institute of Technology, Bengaluru, Karnataka - 560054
* **Corresponding Author Email:** pavitha@msrit.edu - **ORCID:** 0000-0003-4895-3612

[2]Assistant Professor, Department of Electronics and Instrumentation Engineering, Dayananda Sagar College of Engineering Bengaluru, Karnataka - 560078
Email: nikhilamsrit@gmail.com - **ORCID:** 0009-0002-6145-4228

[3]Assistant Professor, Department of Electronics and Communication Engineering, Ramaiah Institute of Technology, Bengaluru, Karnataka - 560054
Email: mamtha.m@msrit.edu - **ORCID:** 0000-0002-7161-0397

Article Info:

DOI: 10.22400/ijcesen.514
Received : 15 October 2024
Accepted : 18 October 2024

Keywords:

Convolutional Neural Network,
DenseNet,
VGG-Net,
InceptionNet,
Grid Artifacts

Abstract:

The digital imaging technique known as Computed Radiography (CR) has transformed the medical imaging industry by providing a number of advantages. It eliminates the need for traditional film-based methods, making it more efficient and convenient. A common issue faced with CR images is the presence of grid artifacts and other pattern artifacts, which can have a significant impact on the quality of the images when viewed on a computer screen, especially if a clinic-grade display is not accessible. This paper presents a novel framework for removing grid line artifacts from X-ray images, which is a critical challenge in medical imaging. The framework proposes a hybrid Deep Grid model that combines a Gaussian band-stop filter with ADAM optimization to produce high-quality, grid-line free X-ray images that are suitable for further analysis and diagnosis. Deep learning (DL) models for instance the Convolutional Neural Network (CNN), DenseNet, VGG-Net, and Fast R-CNN were utilized to classify images, and the grid-by-grid removal of grid lines in the image was performed. The proposed framework achieved a high accuracy rate of 98% in eliminating grid line artifacts from X-ray images, demonstrating its possibility for a big improvement the accuracy and reliability of diagnostics for medical based on X-ray images.

1. Introduction

The transition from conventional analog systems to digital radiographic (DR) systems, which offer customizable signals and higher image quality, has revolutionized medical diagnostics. Even with these advancements, grid artifacts can still appear in DR pictures when anti-scatter grids are used to boost contrast [1–6]. Gridline artifacts may outcome of the use of anti-scatter grids, which can make it difficult to accurately diagnose patients and interpret images [7–18]. The complexity of the imaging process places a limit on the gridline artifact mitigation strategies now in use. To respond to this problem, we have developed a novel framework which uses Hybrid Deep Learning techniques in the elimination of gridline artifacts from X&Y images. Digital twin and container network technology, in particular for Internet of Things applications, are also integrated into the system to improve its capabilities. In order to ensure optimum performance, the digital twin provides real time monitoring and predictive maintenance of the imaging system [19-20]. Deep learning models can be deployed rapidly and effectively through the use of container network technology, which enhances adaptability and integration [21-22]. A Gaussian band-stop filter and ADAM optimization are combined in the proposed Hybrid Deep Learning model to produce high-quality X-ray images that are free of grid-line artifacts and suited for precise analysis and diagnosis [23–24]. We use deep learning models like CNN, DenseNet, VGG-Net, and InceptionNet

to accomplish grid-by-grid removal and identify X-ray pictures. Furthermore, we deal with different kinds of Xray noise that can affect the quality of an image, for example quantum noise, e.g. electrical noise, structure noise, scatter radiation and movement artifacts [25-37]. In order to improve image clarity and diagnose accuracy, it is essential that you understand and mitigate these types of noise. The integration of digital twins and container networks represents a significant benefit for our framework, which is in the process of improving Xray radiography in the healthcare sector. The Digital Twin ensures a constant improvement of the picture quality and system performance by allowing real time monitoring, preventive maintenance or adaptive optimization. Our approach is well suited to medical imaging applications that are connected to the Internet of Things, thanks to a container network technology enabling rapid integration and deployment. With a view to enhancing image quality, improving diagnosis accuracy and expanding possibilities for the use of health care applications, it is expected that this framework will have important effects in healthcare imaging and X ray radiography. We can contribute to a wider set of medical diagnostics with an emphasis on the Internet of Things through research that addresses gridline artifact and other Xray noise sources, thereby giving rise to new kinds of innovation in this vital area.

In the domain of X-ray imaging, various forms of noise can have adverse effects on the quality and clarity of the acquired images. These noise types originate from different sources and exhibit distinct characteristics. Here, I will provide a concise overview of some common varieties of X-ray noise:

1. Quantum Noise: Quantum noise, sometimes referred to as statistical noise or photon noise, is a natural part of X-ray imaging. It results from the stochastic interactions of X-ray photons with the detector and the patient's body. Following a Poisson distribution, quantum noise can lead to image artifacts and reduced image quality, particularly in scenarios involving low radiation doses [38].
2. Electronic Noise: Electronic noise emerges during signal acquisition and processing stages. It can stem from diverse sources such as detector electronics, amplifiers, analog-to-digital converters, and transmission lines. Random variations in pixel values characterize electronic noise, which can impair image clarity and contrast [39].
3. Structured Noise: Structured noise refers to patterns or artifacts introduced into X-ray images due to various factors. These factors may include mechanical imperfections, external interference, calibration issues, or non-uniform detector responses. Streaks, lines, grid patterns, or irregularities in the image can manifest as structured noise, compromising the diagnostic quality [40].
4. Scatter Radiation: Scatter radiation occurs when X-ray photons interact with tissues and change their trajectory. These scattered photons reach the detector, contributing to image degradation by reducing contrast and introducing a hazy appearance. Scatter radiation can be reduced by using methods like post-processing algorithms or anti-scatter grids [41].
5. Motion Artifacts: Motion artifacts arise when there is patient or equipment motion during the X-ray exposure. They result in blurred or distorted images, making accurate interpretation of diagnostic information challenging. Strategies such as immobilization, shorter exposure times, or motion compensation algorithms can help minimize motion artifacts [42].

The characteristics and impact of noise can differ based on the specific imaging system, patient factors, and imaging protocols employed. Addressing and reducing these noise types are vital for enhancing the quality and reliability of X-ray images, thereby enabling more precise diagnosis and treatment. When an anti-scatter grid is used during picture acquisition, a particular kind of structured noise known as "grid line artefacts" may appear in X-ray images. Thin lead strips or septa positioned across the patient and the X-ray detector make up an anti-scatter grid. By absorbing or rerouting scattered photons, it aims to lessen the impact of scattered radiation on image quality [43].

Grid line artifacts become visible as grid-like patterns that overlay the X-ray image. These patterns can manifest as alternating dark and light lines or grid lines. The presence of grid line artifacts can significantly degrade the quality of the image for diagnostic purposes, as they can obscure important anatomical details and mimic pathological findings. Several factors contribute to the occurrence of grid line artifacts:

- Grid misalignment: Grid line artefacts may arise from improper anti-scatter grid alignment with respect to the X-ray beam. Inaccurate placement of the grid or an angle between the grid's orientation and the X-ray beam might cause misalignment.
- Grid cutoff: Grid cutoff occurs when the lead strips of the grid obstruct X-ray photons, leading to incomplete exposure of the detector. This can happen if the X-ray tube is not properly aligned with the grid, causing the grid lines to block some of the primary radiation.

- Moiré effect: The moiré effect can contribute to grid line artifacts when there is an interference pattern between the grid lines and the pixel structure of the X-ray detector. This effect can occur if the grid lines and the pixel pitch of the detector are not appropriately matched.

To minimize or eliminate grid line artifacts, precise alignment and positioning of the grid are essential. Careful arrangement of the X-ray tube, grid, and detector can help mitigate grid cutoff and reduce the likelihood of artifacts. Furthermore, the use of grids with higher frequencies (finer lead strips) can decrease the visibility of grid lines and mitigate their impact on the image. Post-processing techniques, such as grid line artifact removal algorithms, can also be employed to mitigate grid line artifacts after image acquisition. These algorithms analyze the grid patterns and utilize image processing methods to suppress or remove the grid lines while preserving the relevant diagnostic information.

The suppression of gridline artifacts in X-ray images is a complex issue that requires a multidisciplinary approach [12-22]. To address this issue, several image processing techniques have been developed, and these approaches can be broadly categorized into trio groups: wavelet domain suppression techniques, frequency domain filtering techniques, and space domain techniques.

- Space domain methods analyze gridline artifacts as per the Gray level information of the image and suppress them in the spatial domain. However, these approaches are limited, in that, the gridline discovery procedure can be influenced by information in the output image, and the traditional gridline suppression procedure may result in blurring of the object image [12-15].
- In order to distinguish gridline signals and imaging objects in the spatial frequency domain, frequency domain filtering techniques make use of the previous information of the picture state. The gridline artifacts can then be suppressed by filtering the relevant frequencies. However, this approach also has its limitations, as suppressing the gridline frequency may reduce the object image information with similar frequencies [16-20].
- Wavelet domain suppression approaches are designed to reserve detailed object information, but are limited by the zero-assignment process, which can cause a ringing outcome in the final image. Additionally, these approaches do not deliver a stopping state for recursive wavelet transformation. [21-22].

X-ray image classification has traditionally relied on conventional methods that involve manual feature extraction and the application of ML methodologies corresponding Random Forest (RF) and Support Vector Machines (SVMs). Though, these approaches often necessitate extensive manual feature engineering and may struggle to effectively represent complex patterns found in X-ray images. A significant change in methodology has resulted from the field's revolution brought about by the progress of DL. DL frameworks like TensorFlow and PyTorch have demonstrated impressive performance across various image classification tasks. These frameworks make use of neural networks' capacity to automatically extract relevant features from unprocessed data, removing the requirement for time-consuming manual feature engineering and making it possible to identify complicated designs. In summary, X-ray picture gridline artefact suppression is a complicated problem that necessitates carefully weighing the benefits and drawbacks of the many image processing techniques. A combination of approaches and techniques may be needed to achieve optimal results, depending on the specific situation. The proposed method for removing gridline artifacts from X-ray images is an autonomous process that involves several stages to enhance its performance. Deep learning method is important and also used in different applications [44-54].

2. Methods

Xray radiographic images play an essential role in medical diagnosis, but the existence of gridline artifacts can be a major influence on image quality. To enhance the standard of the image for additional diagnostic analysis, here we deploy an innovative methodology that will autonomously identify and remove gridline artifacts from Xray images. This will be achieved by using the Digital Twin and Container Networking Technologies for integration of Internet of Things technologies, in order to ensure that the proposed technique is performing better than before (figure 1). The proposed methodology is set out in the following order:

- A set of xray images is fed to stateoftheart deep learning models, including CNN.NET, VGGNet and the Inception Network in order to classify them into two categories: Dense Lines with Grid artifacts and No Grid artifacts
- Images identified with grid-line artifacts are saved and subsequently processed for grid-line elimination.
- The dense net architecture then receives the saved grid-line-present radiography images and applies a brand-new, improved hybrid deep grid model (GBS-ADAM). To eliminate grid lines in

the resulting photos, this customized activation function combines Gaussian band-stop filters with ADAM optimization.

- The clean, noise-free radiographical images with no grid-line artifacts are kept in a separate folder.
- These radiographical pictures with the grid-line artifacts removed are accessible for additional analysis and user-specific requirements.

We gathered a dataset of almost 3000 radiographical pictures, including COVID lung X-rays, pneumonia lung X-rays, and bone fracture X-rays, from a variety of online sources, including Kaggle and the UCI repository, in order to assess the suggested method. Combinations of photos with and without grid-line artifacts are included in the dataset. About 2000 photographs include grid-line artifacts, while 1000 images were given the grid lines manually removed using Photoshop, making up the category of clean images. The "stratified random sampling" method was used to divide the dataset into training and testing sets, guaranteeing an equivalent distribution of various classes across both sets for a thorough evaluation and generalization of the classification model.

The use of the latest deep learning models, e.g. CNN, DenseNET, VGGnet and InceptionNet, is made for classification of images. To carry out classification, the proposal uses a method of split and conquer to select the most accurate model. Images that can be grouped according to gridlines and with no gridline are generated from the best accuracy model results. Subsequently, an additional assessment is carried out on the images with grid lines.

Our methodology shows an innovative approach to the removal of grid artifacts from Xray radiographic images, using Digital Twin and container network technologies for Internet of Things applications. The Digital Twin ensures real time monitoring and predictive maintenance of the Imaging System, while container Network technology allows effective and scalable deployment of a deep learning model to increase system performance. The aim of this approach is to significantly increase the quality of Xray images in order to facilitate more accurate diagnosis, which would contribute to advancing medical technology through use of internet of things enabled imaging.

2.1 Data Preparation.

In preparation for deep learning, all the sample images were standardized to a uniform size of 224 x 224 pixels. Additionally, data normalization was applied to enhance the learning capabilities of the system. With these steps taken, the dataset was deemed ready for input into various advanced deep learning methodologies and to commence the training process. During the training of a DL methodology for X-ray image classification, it is critical to address potential biases associated with the manual pixel-shift (PS) based noise removal technique. Manual interventions, such as PS-based noise removal, can unintentionally introduce biases that distinguish PS images from non-PS images based on subjective perceptions of image quality and individual operations. These biases can significantly impact the model's performance and generalizability. Moreover, manual operations involved in PS-based noise removal can introduce additional variations or artifacts into the images. If not carefully controlled, these variations can create differences between PS and non-PS images that are dissimilar to the occurrence of noise. Consequently, the methodology may learn to associate specific visual cues or artifacts with the presence or absence of PS rather than accurately identifying and classifying noise patterns. In order to address the issues, autonomous deep learning methods are utilized.

2.2 Convolutional Neural Network (CNN).

The CNN, also identified as ConvNet, is a kind of NN that is primarily utilized in image classification as well as in recognizing speech. A CNN's architecture is made up of several layers. The layers in the CNN receive the input, and then process it to convert the data from the image, and then the processed data are passed to the successive layers. This kind of processing is called convolution. In each convolution process, the number of filters to be utilized should be properly defined. Filters are image processing tools that identify specific patterns in an image, such as edges, shapes, curves, objects, textures, or colors. The complexity of the detected patterns is directly proportional to the depth of the filter. These filters are implemented as small matrices, known as image kernels, that are applied to an entire image. Convolution and pooling layers are often used in conjunction with filters, where the pooling layer helps to down sample the input image, reducing its dimensionality by retaining the most relevant features in subregions. The stride is the number of pixels that are moved across the input matrix during the filtering process. When stride is set to 1, the filter advances one pixel at a time; when stride is set to 2, the filter advances two pixels at a time. Large photos can be processed more effectively by using larger strides and filter sizes. Figure 2 illustrates the CNN architecture that was used for both Grid and non-Grid artefact categorisation. Convolutional,

pooling, and Fully Connected Layers (FCL) are the three different layers that make up the suggested CNN framework. RGB images with dimensions of 224 × 224 × 3 are fed into the framework. The initial layer is the convolutional layer, which uses filters, also referred to as "kernels," with a size of (3 × 3).

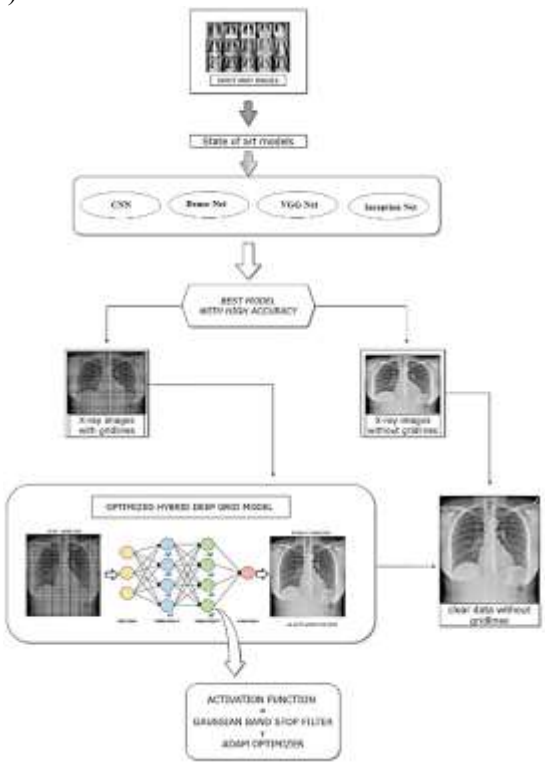

Figure 1. *Proposed Architecture*

These filters serve as feature identifiers and extract lower-level features such as edges and curves. By adding additional convolutional layers, the model can extract deep features from images and determine their complete characteristics. The filter achieves a convolution process with a sub portion of the image, which is referred to as the "receptive field." The parameters of the filter, also known as weights, are learned through training. The spatial dimension of the input volume decreases with an increase in the stride value, which determines the amount by which the filter is shifted. Padding is employed to keep the output dimensional volume equal to the input in order to get around this. To extract various features, the convolutional layer employs many filters. To include a nonlinear to the linear operation, the convolutional output is given the activation-function ReLU (Rectified-Linear Unit). Subsequent two convolutional layers, the max-pooling layer is used to minimise the input's spatial dimensions by utilising the maximum receptive field value with a stride of two and a filter of size 2 2. Then, using a threshold-value of 0.251, the dropout layer is used to randomly eliminate some activations in order to avoid overfitting. The flattened layer transforms the 2D feature map into a 1D feature vector, which the FCL then uses for classification. The final output layer uses the "softmax" activation to forecast the class label of grid artefacts against nongrid artefacts. The FCL is made up of 64 neurones. Table 1 shows the specifics of the layer.

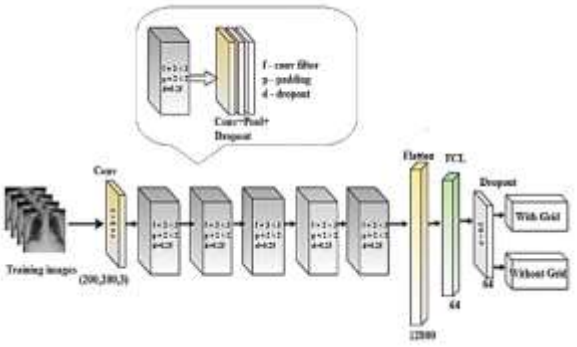

Figure 2. *CNN architecture*

Table 1: *Layers of CNN*

Layer	Size of the Filter	Size of the Pool	Stride	Padding	Total filters	Dropout threshold	Activation function
Conv2D	3 X 3	-	2	Valid	32	-	Relu
Conv2D	3 X 3	-	2	Valid	128	-	Relu
MaxPooling2D	-	2 X 2	2	-	-	-	-
Dropout	-	-	-	-	-	0.25	-
Conv2D	3 X 3	-	2	Valid	64	-	Relu
MaxPooling2D	-	2 X 2	2	-	-	-	-
Dropout	-	-	-	-	-	0.25	-
Conv2D	3 X 3	-	2	Valid	128	-	Relu
MaxPooling2D	-	2 X 2	2	-	-	-	-
Dropout	-	-	-	-	-	0.25	-
Conv2D	3 X 3	-	2	Valid	512	-	Relu
MaxPooling2D	-	2 X 2	2	-	-	-	-
Dropout	-	-	-	-	-	0.25	-
Conv2D	3 X 3	-	2	Valid	512	-	Relu
MaxPooling2D	-	2 X 2	2	-	-	-	-
Dropout	-	-	-	-	-	0.25	-
Flatten	-	-	-	-	-	-	-
FCL	-	-	-	-	64	-	Relu
Dropout	-	-	-	-	-	0.25	-
FCL	-	-	-	-	2	-	Sigmoid

DenseNet. The DenseNet201 architecture consists of a 201-layer dense connected convolutional network. The network comprises four densely linked blocks and transition layer pooling that connects these blocks uniformly [27-28]. The network can gain additional input features and improve feature reuse efficiency by employing a structure of Batchnorm + ReLU + 3 x 3 Conv. In doing so, the vanishing gradient problem would be partially mitigated and the total amount of network parameters would be reduced [29].

VGGNet16. The VGG network structure more especially, the VGG16 model is another method employed in this investigation. The VGG16 architecture is intended to improve the network's performance while deepening it. A tiny convolutional kernel, a tiny pooling kernel, and the ReLU activation function make up the VGG16 model's basic module. The network structure consists of five convolutional layers, three fully linked layers, and a final softmax output layer. All hidden layers use the ReLU activation function, and the layers are separated via max pooling [30]. The ease of the VGG network building is one of its primary advantages. After the $7 \times 7 \times 512$ feature map is fully connected, the softmax activation function is used to achieve the final recognition results for the three objects.

Inception Net. The Deep CNN (DCNN) methodology known as GoogLeNet, created by scientists at Google as part of their InceptionNet design, takes on the problem of boosting network depth while preserving effectiveness in processing. The "Inception module," one of its ground-breaking features, makes it possible to effectively retrieve multi-scale information from input photos. The fundamental idea behind the Inception module is to conduct concurrent convolutions with various filtering sizes, then combine the results. By enabling the network to record both local and global characteristics at different scales, this method improves the network's capacity for distinguish intricate trends and structures in visuals. The Inception module includes a bottleneck layer that uses a 1x1 convolutional algorithm to minimize input dimensionality. It is complemented by alternating branches made up of convolutions of various sizes (e.g., 1x1, 3x3, 5x5). The component also includes max pooling algorithms to gather geographical information and reduce spatial dimensions. Lastly, all branch outcomes are combined along the channel's length to provide the module's final outcome. Another of the InceptionNet architecture's significant benefits is its effectiveness in computing. The architecture decreases processing needs while successfully utilizing network parameters by implementing 1x1 convolutions. As a consequence, deeper networks are able to be built using a parameter count similar to older models, leading to enhanced representational learning skills. InceptionNet has outperformed other picture classification algorithms in a variety of responsibilities, notably the extremely renowned ImageNet Large-Scale Visual Recognition Challenge (ILSVRC). Its effectiveness can be due to its ability to collect global as well as local features, effective networking parameter usage, and deep design that enables nested feature learning. The final output produced by this process is the classification of the image as either containing grid artifacts or not containing grid artifacts.

The proposed framework compares the results from various state-of-the-art models and automatically selects the most accurate one. The best-trained model is then used to test images and classify them into two categories: images with "Grid Artifacts" and images without "Grid Artifacts." The classified images with "Grid Artifacts" are further processed by the framework.

Grid Line Detection and Removal Module. The images classified as "Grid Artifacts" are then processed through the proposed DenseNet architecture with a custom activation function. The activation function is based on a novel hybrid deep grid model, which combines a Gaussian band stop filter with ADAM optimization (GBS-ADAM). The Adam optimizer, which is derived from the phrases Adaptive Moment Estimation, incorporates the benefits of the AdaGrad and RMSProp optimization techniques. Adam offers rapid and successful optimization through preserving variable learning rates for specific parameters.The Adam optimizer continually changes its learning rate for every parameter throughout training depending on the anticipated first and second values of the gradients. This variable learning rate technique speeds up closure and enhances the methodology ability to manage various types of data and complicated topologies. Using the Adam optimizer's skills, the model may effectively adjust its parameters during the tuning process, resulting in improved efficiency. This optimized hybrid model optimizes the images grid by grid, effectively removing the grid lines in the final output images.

The process of recursive wavelet decomposition [37] continues until a subimage containing the main gridline signal is created by the gridline discovery unit. Gridline artifacts are characteristically characterized by line-shaped shades. To determine if the gridline is the primary signal in the image in question, statistical-texture features can be employed. Based on the picture Grey Level Co-

Occurrence Matrix (GLCM), [35] has identified 14 statistical-texture characteristics [37], although these features include duplicate information. However, according to [36], only four of these features correlation, contrast, energy, and inverse moment are uncorrelated. For this reason, this study decided to define the intensity of gridline artefacts using correlation and contrast [37]. The spatial GLCM is constructed by calculating the frequency at which a pixel with intensity (gray-level) value k appears in a precise spatial relationship with a pixel with value l. To describe the spatial relationship, an angular relationship and a distance d are needed. Assuming that the gridline-artifacts are parallel to the image's axis, two angular relations of 0° and 90° were selected for this study in order to compute the consistent spatial GLCMs, which are represented as P(d, 0°) and P(d, 90°), respectively. The vertical GLCM is P(d, 90°), and the horizontal GLCM is P(d, 0°) [37].

Equation 1 below shows the results of the computations used to determine the correlation [37], which characterises pixel correlation in a particular angle of the image.

$$Correlation = \sum_{k=0}^{G-1}\sum_{l=0}^{G-1}\frac{p_{kl}(k-\mu_k)(l-\mu_l)}{\sigma_i\sigma_j} \quad (1)$$

where $\mu_k = \sum_{k=0}^{G=1}\sum_{l=0}^{G-1}(p_{kl} * k)$, $\mu_k = \sum_{k=0}^{G-1}\sum_{l=0}^{G-1}(p_{kl} * l)$, $\sigma_k = \sqrt{\sum_{k=0}^{G-1}\sum_{l=0}^{G-1}(p_{kl} * (k-\mu_k)^2)}$, $\sigma_l = \sqrt{\sum_{k=0}^{G-1}\sum_{l=0}^{G-1}(p_{kl} * (l-\mu_l)^2)}$

The GLCM is also used to calculate contrast [37], which indicates the level of picture clarity and texture groove depth in the direction. The results are shown in Equation 2 below.

$$Contrast = \sum_{k=0}^{G-1}\sum_{l=0}^{G-1} p_{kl}|k-l^2| \quad (2)$$

Gaussian band-stop filter. Gridline artefacts in X-ray images are suppressed by applying a Gaussian band-stop filter to the image's columns. The following Equation 3 shows the formula.

$$B(u) = 1 - e^{-\frac{1}{2}(\frac{u-\mu}{\sigma})^2}, u = 1, \dots, M \quad (3)$$

where the actual frequency of the image's gridlines is represented by μ=p'u. The maximum value in the power spectrum is used to choose the μ value. The σ value is calculated using interval values [$p'u$ – *0.50 * W, $p'u$ + 0.50 * W]*, wherein W is the width of the wave peak in two or multiples. In order to create a gridline-free image (I′c(x,y)), the filter is intended to exclude the gridline signal (Ic(x,y)) from the image. This processed image is then blended with a pyramidal Discrete Wavelet Transform (DWT) to create the final restored image free of gridline artefacts. To sum up, the method needs an input X-ray image with gridlines (I(x,y)), the number of pixels in the image, the direction of gridline artefacts (d), and the number of gridlines per centimetre (fg). Procedure to eliminate gridlines in X-ray imagery using novel hybrid Deep Grid Model involves a combination of a Gaussian band-stop filter and Adam optimization. The steps are as follows:

- Initialization: Gridline artifacts [37] in the input X-ray picture (I(x,y)), frequency of gridlines per cm (fg), pixel resolution (R_s), and gridline artifact direction (d).
- Gaussian Band-stop Filter Application: Apply Gaussian band-stop filter to columns of the X-ray image to eliminate the gridline signals and produce the (I′$_c$(x,y)).
- Adam Optimization Utilization: To make the (I′c(x,y)) better, apply the Adam optimisation technique. To minimise the inaccuracy among the original X-ray image and the gridline-free image, the Adam optimisation technique uses gradient descent to modify the filter settings.
- Inverse DWT Implementation: To create the final restored X-ray image devoid of gridline artifacts, an Inverse DWT [37] is applied to the optimized gridline-free image.
- Output: The final product is the restored X-ray image free of gridline artifacts.

The mean squared error (MSE) of the unfiltered image and the filtered image determines the stopping point for the Gaussian filter in the suggested study. The MSE is a statistic used to evaluate the difference between two images, having a lower MSE suggesting greater similarity and better elimination of gridline aberrations. The evaluation function considered for this study is also MSE. At every stage of the filtering procedure, the MSE is determined to establish the threshold for terminating the Gaussian filter. The MSE among the original image and the filtered image must be lower than the threshold in order for the threshold to be met. This minimizes the introduction of extra noise while ensuring that the filtering process ends when the appropriate level of artifact removal has been reached. The suggested method tries to achieve a balance between efficiently removing gridline artifacts and maintaining the entire quality and authenticity of the X-ray images by using the MSE as the halting criteria. This method ensures the best outcomes in terms of artifact elimination and image quality by providing an objective statistic to guide the filtering procedure's termination based on the obtained similarity among the original and filtered images. By combining the Gaussian band-stop filter and Adam optimization,

the aim is to effectively eliminate the gridline artifacts and produce high-quality X-ray images. The proposed hybrid deep grid algorithm is detailed below.

Algorithm: Hybrid Deep Grid

INPUT: Gridline artifacts in the input X-ray picture (I(x,y)), frequency of gridlines per cm (fg), R_s, and d.

OUTPUT: Restored X-ray image without gridline artifacts

1. Initialize $B(u)$ [37] parameters
2. For every column in the X-ray image:
2.1 Apply $B(u)$ to attain (I'_c(x,y))
3. Initialize Adam optimization algorithm parameters
4. Repeat until convergence:
4.1 Compute gradient of error between original X-ray image and gridline-free image
4.2 Update filter parameters using Adam

3. Results and Discussion.

A collection of 3000 radiography images was gathered for this investigation from a variety of online sources. The images include X-rays of COVID lungs, pneumonia lungs, and bone fractures, both with and without gridline artifacts. Of the 3000 images, 2000 had gridline artifacts, and 1000 were manually processed using Photoshop to remove the gridlines. These 1000 images were considered as the reference category. The dataset was split 80:20, with 600 photos used for testing and 2400 images used for training. A sample of the images used is represented in Figure. 3.

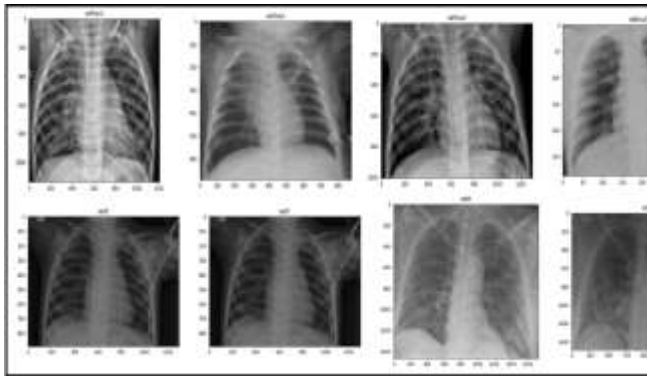

Figure 3*. Sample of Image Collected*

To classify the images, advanced DL methodologies for instance the CNN, DenseNet, VGG-Net, and InceptionNet were used. The sample training accuracy and validation accuracy for the CNN and the training loss and validation loss are depicted in Figure. 4a and 4b. Comparison consequences of the advanced methodologies such as CNN, DenseNet, VGG-Net, and InceptionNet are depicted in Table 2. The comparative findings of cutting-edge models' accuracy, precision, F1 score, specificity and sensitivity are depicted in Figure. 5a. Figure 5a depicts that the accuracy of the convolutional neural network is 1.14%, 3.76%, and 1.95% higher than that of DenseNet, VGG-Net and InceptionNet, respectively.

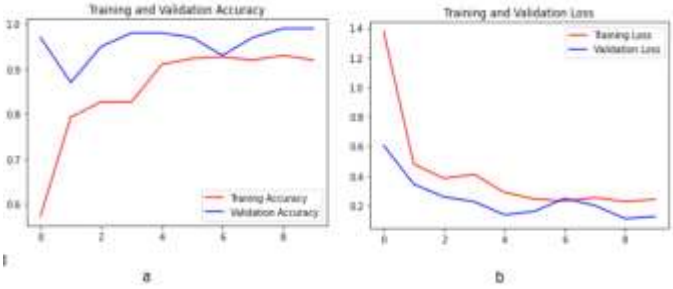

Figure 4. *a. Training Accuracy and Validation Accuracy for CNN b. Training and Validation Loss for CNN*

Table 2. *Comparison results of the state-of-the-art models*

State of Art Models	Accuracy in %	F1 Score in %	Specificity in %	Precision in %	Sensitivity in %
CNN	92.64	95.8	78.4	96.6	95.00
DenseNet	91.5	93.94	74.19	94.80	92.30
VGG-Net	88.64	93.43	73.49	95.66	91.02
InceptionNet	90.45	97.56	95.66	94.24	94.68

The F1 score of InceptionNet is 1.76%, 3.62% and 4.13% higher than that of CNN, DenseNet and VGG-Net, respectively. Similarly, the specificity of InceptionNet is 17.26%, 21.47% and 22.17% higher than that of CNN, DenseNet and VGG-Net, respectively. The precision score of the CNN is 1.8%, 0.94%, and 2.36% higher than that of DenseNet, VGG-Net and InceptionNet, respectively. The sensitivity score of CNN also performs higher by 2.7%, 3.98%, and 0.32% than DenseNet, VGG-Net and InceptionNet, respectively. From the results, it is clear that CNN outperforms the results of DenseNet, VGG-Net and InceptionNet, and the framework as per the accuracy value, it chooses the CNN as the best model, and the images classified by CNN are considered for further processing. The ROC curve of the CNN model is represented in Figure. 5b, which details that the true positive rate is gradually higher than the negative rate. The outcome of the prediction of the CNN are illustrated in Figure. 6, which shows that the positive prediction is higher than

the negative prediction. In order to enhance the total performance of this framework, digital twin and container networks have been instrumental in enabling integration into the Internet of Things by improving image quality and diagnoseability. The digital twin's real time monitoring and predictive maintenance, as well as its adaptive optimization will make it more reliable and effective in the field of imaging. Moreover, the container network technology allows seamless deployment of deep learning models across a variety of health care environments and makes it possible to adapt them for several kinds of IoT enabled environment.

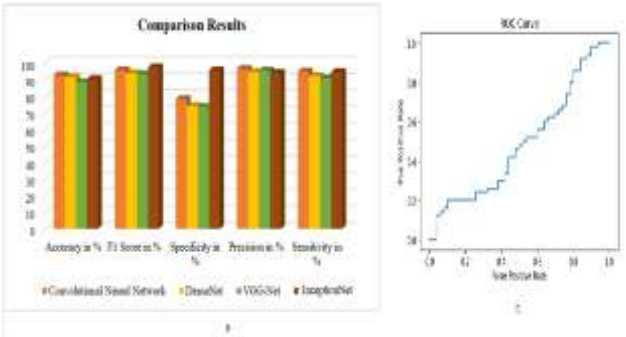

Figure 5*. a. Comparison results of the state-of-the-art, b. ROC curve of the CNN*

The proposed hybrid deep grid model involves a two-step process for removing gridline artifacts from X-ray images. First, the images are classified into those that contain grid artifacts and those that do not. For this classification task, a advanced DL methodologies for instance CNN, DenseNet, VGG-Net, or InceptionNet are chosen based on their performance on a dataset of radiographical images. Once the images with grid artifacts have been identified, they are processed by the hybrid deep grid model. The model performs a grid-by-grid analysis of the image, considering each subimage separately, and applies a customized activation function that combines a Gaussian band-stop filter and Adam optimization. The purpose of this combination is to remove the gridline signals effectively and produce a high-quality gridline-free image as the final output.

The hybrid deep grid model is capable of refining grid lines of any angle, including horizontal, vertical, and diagonal grid lines. The result of the model's processing is an X-ray image free of grid artifacts, as shown in Figure. 7. The proposed framework outputs these gridline-free X-ray images as the result. Finally, the output image produced by the proposed framework is completely free of grid lines and can be used for further classification and analysis. However, several limitations are worth considering. Acquiring a large and diverse dataset of X-ray images can be challenging due to privacy concerns and the need for collaboration with medical institutions. Additionally, training deep learning models often necessitates significant computing power and resources. Developing the custom activation function and optimizing the grid removal process also presented its own set of challenges. The study analyzes the performance of various DL methodologies for image classification. CNN achieved the highest accuracy (92.64%) compared to DenseNet, VGGNet, and Fast R-CNN. For grid removal, the framework employs a customized activation function that combines filtering and optimization techniques. The comparison of the deployed methodology along with additional existing models like CNN [28], deep CNN [29], 3D CNN [30], UNet with band patch [31] are performed and the comparison ablation studies are represented in Table 3. From Table 3, it is understood that the proposed model holds higher accuracy than other related studies.

4. Conclusion

The proposed framework that combines the Gaussian band-stop filter with the ADAM optimization algorithm has demonstrated its effectiveness in removing grid line artifacts from

Table 3. *Comparison of accuracy of the Proposed model with the related works*

Models	**Techniques**	**Accuracy(in %)**
Kim [28]	CNN with learning data construction	96
Lopes [29]	Deep CNN	97
Duffy [30]	3D CNN	97.5
Okamoto [31]	UNet with band patch	96.5
Proposed Model	Hybrid deep grid model	98

.

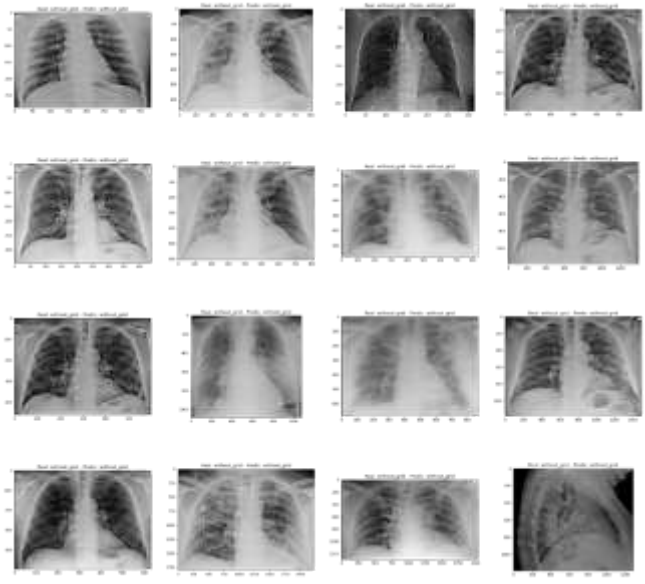

Figure 6*. Predicted Results of CNN*

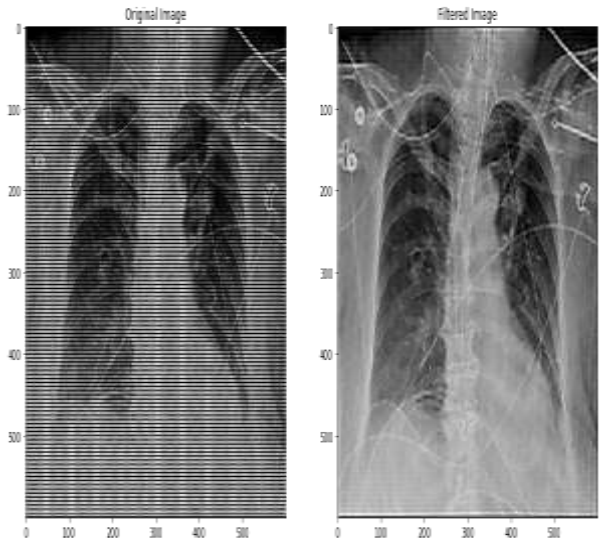

Figure 7. *Final output of the hybrid deep grid model*

X-ray images. The implementation of this framework addresses a significant challenge faced in medical imaging, which is producing clear and unobstructed images for accurate diagnosis. The use of DL methodologies like the CNN, DenseNet, VGG-Net, and Fast R-CNN for image classification and the grid-by-grid removal of grid lines in the image have shown promising results. The output of the framework is a high-quality, grid-line free X-ray image that can be used for further analysis and diagnosis. An accuracy rate of 98% is achieved through the deployed framework in removing grid-line artifacts in X-ray images. All things considered, the suggested framework could greatly increase the accuracy of and reliability of medical diagnoses based on X-ray images. Thus the proposed model demonstrates the efficacy of conjucting Gaussian band stop filter with ADAM optimizer for removing grid-lines in radiographical images. However, a large dataset with the proposed model's exploration with various artifacts would strength the research's generalizability. Further the research is improved by expanding the dataset with more number of images for improving the generalizability along with addressing other different variants of artifacts and its corresponding clinical impacts by exploring real-time diagnosis.

Author Statements:

- **Ethical approval:** The conducted research is not related to either human or animal use.
- **Conflict of interest:** The authors declare that they have no known competing financial interests or personal relationships that could have appeared to influence the work reported in this paper
- **Acknowledgement:** The authors declare that they have nobody or no-company to acknowledge.
- **Author contributions:** The authors declare that they have equal right on this paper.
- **Funding information:** The authors declare that there is no funding to be acknowledged.
- **Data availability statement:** The data that support the findings of this study are available on request from the corresponding author. The data are not publicly available due to privacy or ethical restrictions.

References

[1]Tanaka, N et al., (2013). Investigation of optimum anti-scatter grid selection for digital radiography: physical imaging properties and detectability of low-contrast signals. *Radiological physics and technology*, 6;54-60.

[2]Gennaro, G. et al., (2007). Grid removal and impact on population dose in full- field digital mammography. *Medical physics*, 34(2);547-555.

[3]Lehnert, T. et al., (2014). Comparative study between mobile computed radiography and mobile flat-panel radiography for bedside chest radiography: impact of an antiscatter grid on the visibility of selected diagnostically relevant structures. *Investigative radiology*, 49(1);1-6.

[4]Veldkamp, W.J., Thijssen, M.A. and Karssemeijer, N., (2003). The value of scatter removal by a grid in full field digital mammography. *Medical Physics*, 30(7);1712-1718.

[5]Shaw, C.C., Wang, T. and Gur, D., (1994). Effectiveness of antiscatter grids in digital radiography: a phantom study. *Investigative radiology*, 29(6);636-642.

[6]Fetterly, K.A. and Schueler, B.A., (2008). Physical evaluation of prototype high-performance anti-scatter grids: potential for improved digital radiographic image quality. *Physics in Medicine & Biology*, 54(2);N37.

[7]Sorenson, J.A., Niklason, L.T., Jacobsen, S.C., Knutti, D.F. and Johnson, T.C., (1982). Tantalum air-interspace crossed grid: design and performance characteristics. *Radiology*, 145(2);485-492.

[8]Robinson, J.D., Ferlic, D., Kotula, F., Ferlic, L., Geise, R.A. and Amplatz, K., (1993). Improved mammography with a reduced radiation dose. *Radiology*, 188(3);868-871.

[9]Gauntt, D.M. and Barnes, G.T., (2006). Grid line artifact formation: A comprehensive theory. *Medical physics*, 33(6 Part1);1668-1677.

[10]Gauntt, D.M. and Barnes, G.T., (2006). A novel technique to suppress grid line artifacts. *Medical physics*, 33(6 Part1);1654-1667.

[11]Yoon, J.W., Park, Y.G., Park, C.J., Kim, D.I., Lee, J.H., Chung, N.K., Choe, B.Y., Suh, T.S. and Lee, H.K., (2007). Reduction of a grid moiré pattern by integrating a carbon- interspaced high precision x-

ray grid with a digital radiographic detector. *Medical physics*, 34(11);4092-4097.

[12]Barski, L.L. and Wang, X., (1999), May. Characterization, detection, and supression of stationary grids in digital projection radiography imagery. *Medical Imaging 1999: Image Display* 3658; 502-519.

[13]Maruyama, T. and Yamamoto, H., (2006), December. Elimination of Gridlines in X-ray Imaging for Mammography. *In IST 2006-2006 IEEE International Workshop on Imagining Systems and Techniques* (pp. 104-109).

[14]Maruyama, T. and Yamamoto, H., (2008), May. Elimination of gridlines in X-ray image. *In 2008 IEEE Instrumentation and Measurement Technology Conference* (pp. 1091-1096). IEEE.

[15]Maruyama, T. and Yamamoto, H., (2011). Elimination of gridlines by using non-linear filter in mammographic image. *IET image processing*, 5(5);457-465.

[16]Barski, L.L. and Wang, X., Eastman Kodak Co, (2001). Method for X-ray antiscatter grid detection and suppression in digital radiography. U.S. Patent 6,269,176.

[17]Belykh, I.N. and Cornelius, C.W., Eastman Kodak Co, (2006). Method for antiscatter stationary grid artifacts detection and attenuation in digital radiographic images. U.S. Patent 7,050,618.

[18]Lin, C.Y., Lee, W.J., Chen, S.J., Tsai, C.H., Lee, J.H., Chang, C.H. and Ching, Y.T., (2006). A study of grid artifacts formation and elimination in computed radiographic images. *Journal of digital imaging*, 19;351-361.

[19]Kim, D.S. and Lee, S., (2011), September. Adaptive grid pattern artifact reduction in radiography imaging based on the significant-signal bandwidth. In 2011 *18th IEEE International Conference on Image Processing* (pp. 1473-1476). IEEE.

[20]Kim, D.S., Lee, S. and Yoon, J.K., (2013), March. Grid artifact reduction based on homomorphic filtering in digital radiography imaging. *In Medical Imaging 2013: Physics of Medical Imaging* (Vol. 8668, pp. 639-647). SPIE.

[21]Takeo, H., Fujifilm Corp, (2008). Method and unit for suppressing a periodic pattern. U.S. Patent 7,336,811.

[22]Sasada, R., Yamada, M., Hara, S., Takeo, H. and Shimura, K., (2003), May. Stationary grid pattern removal using 2D technique for moiré-free radiographic image display. *In Medical Imaging 2003: Visualization, Image-Guided Procedures, and Display* (Vol. 5029, pp. 688-697). SPIE.

[23]Karthiga M, Shanthi V, and Sountharrajan S, (2022). Hybrid Optimized Convolution Neural Network for Efficient Classification of ECG Signals in Healthcare Monitoring, *Biomedical Signal Processing and Control*, 76;103731.

[24]R. Arthi and S. Harini, (2018). A Survey of Deep Convolutional Neural Network Applications in Image Processing, *Computer Science Computer Vision and Pattern Recognition* 8(7);185-190. https://doi.org/10.1007/s10462-020-09825-6

[25]Vinayakumar R., Soman KP., and Prabhaharan Poornachandran., (2019). A Comparative Analysis of Deep Learning Approaches for Network Intrusion Detection Systems (N-IDS): *Deep Learning for N-IDSs*, 11(3);65-83.

[26]G. Anitha and S. Baghavathi Priya, (2022). Vision based real time monitoring system for elderly fall event detection using deep learning, *Computer Systems Science and Engineering*, 42(1);87–103.

[27]M. Lin, Q. Chen, and S. Yan, Network in network, in: *2nd Int. Conf. Learn. Represent. ICLR 2014 - Conf. Track Proc.*, 2014.

[28]Li, W., Liu, K., Yan, L., Cheng, F., Lv, Y. and Zhang, L., (2019). FRD-CNN: Object detection based on small-scale convolutional neural networks and feature reuse. *Scientific reports*, 9(1);1-12.

[29]Li, W., Liu, K., Yan, L., Cheng, F., Lv, Y. and Zhang, L., (2019). FRD-CNN: Object detection based on small-scale convolutional neural networks and feature reuse. *Scientific reports*, 9(1);1-12.

[30]K. Simonyan, A. Zisserman, Very deep convolutional networks for large-scale image recognition, in: *3rd Int. Conf. Learn. Represent. ICLR 2015 - Conf. Track Piroc.*, 2015.

[31]Girshick, R. and Donahue, J., Trevor DARRELL a Jitendra MALIK. Rich feature hierarchies for accurate object detection and semantic segmentation. *In Proceedings of the IEEE Computer Society Conference on Computer Vision and Pattern Recognition* (pp. 580-587).

[32]Gu, C., Lim, J.J., Arbeláez, P. and Malik, J., (2009), June. Recognition using regions. *In 2009 IEEE Conference on computer vision and pattern recognition* (pp. 1030-1037). IEEE.

[33]Uijlings Jasper, R.R. and Van De Sande Koen, E.A., (2013). Gevers Theo, and Smeulders Arnold WM,". Selective search for object recognition", *International journal of computer vision*, 104(2);154-171.

[34]Maheshwari, R.U., Kumarganesh, S., K V M, S. et al. (2024). Advanced Plasmonic Resonance-enhanced Biosensor for Comprehensive Real-time Detection and Analysis of Deepfake Content. *Plasmonics*. https://doi.org/10.1007/s11468-024-02407-0

[35]Maheshwari, R. U., Paulchamy, B., Arun, M., Selvaraj, V., & Saranya, N. N. (2024). Deepfake Detection using Integrate-backward-integrate Logic Optimization Algorithm with CNN. *International Journal of Electrical and Electronics Research*, 12(2), 696-710.

[36]Maheshwari, R. U., & Paulchamy, B. (2024). Securing online integrity: a hybrid approach to deepfake detection and removal using Explainable AI and Adversarial Robustness Training. *Automatika*, 65(4), 1517-1532.

[37]Sood, K., Dhanaraj, R. K., Balusamy, B., Grima, S., & Uma Maheshwari, R. (Eds.). (2022). Big Data: A game changer for insurance industry. *Emerald Publishing Limited*.

[38]Janarthanan, R., Maheshwari, R. U., Shukla, P. K., Shukla, P. K., Mirjalili, S., & Kumar, M. (2021). Intelligent detection of the PV faults based on

artificial neural network and type 2 fuzzy systems. *Energies*, 14(20), 6584.

[39]Appalaraju, M., Sivaraman, A. K., Vincent, R., Ilakiyaselvan, N., Rajesh, M., & Maheshwari, U. (2021). Machine learning-based categorization of brain tumor using image processing. In Artificial Intelligence and Technologies: *Select Proceedings of ICRTAC-AIT 2020* (pp. 233-242). Singapore: Springer Singapore.

[40]Sasikala, S., Sasipriya, S., & Maheshwari, U. (2022, March). Soft Computing based Brain Tumor Categorization with Machine Learning Techniques. *In 2022 International Conference on Advanced Computing Technologies and Applications (ICACTA)* (pp. 1-9). IEEE.

[41]Zaitsev, Maxim, Julian Maclaren, and Michael Herbst. (2015). Motion artifacts in MRI: A complex problem with many partial solutions. *Journal of Magnetic Resonance Imaging* 42(4);887-901.

[42]Lin, Chih-Yang, Wen-Jeng Lee, Shyh-Jye Chen, Ching-Hwa Tsai, Jei-Han Lee, Chia-Hung Chang, and Yu-Tai Ching. (2006). A study of grid artifacts formation and elimination in computed radiographic images. *Journal of digital imaging* 19;351-361.

[43]Cochran, William G. Sampling techniques. John Wiley & Sons, 1977.

[44]Priti Parag Gaikwad, & Mithra Venkatesan. (2024). KWHO-CNN: A Hybrid Metaheuristic Algorithm Based Optimzed Attention-Driven CNN for Automatic Clinical Depression Recognition . *International Journal of Computational and Experimental Science and Engineering*, 10(3);491-506. https://doi.org/10.22399/ijcesen.359

[45]Rakesh Jha, & Singh, M. K. (2024). Analysing the Impact of Social Influence on Electric Vehicle Adoption: A Deep Learning-Based Simulation Study in Jharkhand, India. *International Journal of Computational and Experimental Science and Engineering*, 10(4);639-646. https://doi.org/10.22399/ijcesen.371

[46]P, P., P, D., R, V., A, Y., & Natarajan, V. P. (2024). Chronic Lower Respiratory Diseases detection based on Deep Recursive Convolutional Neural Network. *International Journal of Computational and Experimental Science and Engineering*, 10(4);744-756. https://doi.org/10.22399/ijcesen.513

[47]M, V., V, J., K, A., Kalakoti, G., & Nithila, E. (2024). Explainable AI for Transparent MRI Segmentation: Deep Learning and Visual Attribution in Clinical Decision Support. *International Journal of Computational and Experimental Science and Engineering*, 10(4);575-584. https://doi.org/10.22399/ijcesen.479

[48]KIRELLİ, Y., & AYDIN, G. (2023). Classification of Histopathological Images in Automatic Detection of Breast Cancer with Deep Learning Approach. *International Journal of Computational and Experimental Science and Engineering*, 9(4), 359–367. Retrieved from https://www.ijcesen.com/index.php/ijcesen/article/view/279

[49]Agnihotri, A., & Kohli, N. (2024). A novel lightweight deep learning model based on SqueezeNet architecture for viral lung disease classification in X-ray and CT images. *International Journal of Computational and Experimental Science and Engineering*, 10(4);592-613. https://doi.org/10.22399/ijcesen.425

[50]Jha, K., Sumit Srivastava, & Aruna Jain. (2024). A Novel Texture based Approach for Facial Liveness Detection and Authentication using Deep Learning Classifier. *International Journal of Computational and Experimental Science and Engineering*, 10(3);323-331. https://doi.org/10.22399/ijcesen.369

[51]AYKAT, Şükrü, & SENAN, S. (2023). Using Machine Learning to Detect Different Eye Diseases from OCT Images. *International Journal of Computational and Experimental Science and Engineering*, 9(2), 62–67. Retrieved from https://www.ijcesen.com/index.php/ijcesen/article/view/191

[52]Achuthankutty, S., M, P., K, D., P, K., & R, prathipa. (2024). Deep Learning Empowered Water Quality Assessment: Leveraging IoT Sensor Data with LSTM Models and Interpretability Techniques. *International Journal of Computational and Experimental Science and Engineering*, 10(4);731-743. https://doi.org/10.22399/ijcesen.512

[53]ÇELİK, M. E. (2023). A Novel Deep Learning Model for Pain Intensity Evaluation. *International Journal of Computational and Experimental Science and Engineering*, 9(4), 325–330. Retrieved from https://www.ijcesen.com/index.php/ijcesen/article/view/274

[54]BACAK, A., ŞENEL, M., & GÜNAY, O. (2023). Convolutional Neural Network (CNN) Prediction on Meningioma, Glioma with Tensorflow. *International Journal of Computational and Experimental Science and Engineering*, 9(2), 197–204. Retrieved from https://www.ijcesen.com/index.php/ijcesen/article/view/210